Electronic Supplementary Information (ESI) for:

Synthesis, Structural, Photophysical, Electrochemical Redox and Axial Ligation Properties of Highly Electron Deficient Perchlorometalloporphyrins and Selective CN^- Sensing by Co(II) Complexes

Nivedita Chaudhri[a], Ray J. Butcher[b] and Muniappan Sankar[a]*

[a]*Department of Chemistry, Indian Institute of Technology Roorkee, Roorkee-247667, India*
[b]*Department of Chemistry, Howard University, Washington, DC 20059, USA*

Contents		**Page No.**
Fig. S1	The ORTEP diagrams showing top views of (a) $CoTPP(NO_2)Cl_7$.MeOH (**1a**.MeOH), (b) $ZnTPP(NO_2)Cl_7$.Py (**1d**.Py) and (C) $NiTPPCl_8$ (**2b**).	3
Fig. S2	The packing diagram of (a) $ZnTPP(NO_2)Cl_7$.MeOH (**1d**.MeOH) and (b) $ZnTPPCl_8$.MeOH (**2b**.MeOH).	3
Fig. S3	Displacement of porphyrin core atoms (in Angstroms) from the mean plane for $CoTPP(NO_2)Cl_7$.MeOH(**1a**.MeOH) (a), $ZnTPP(NO_2)Cl_7$.Py (**1d**.Py) and $NiTPPCl_8$ (2b) (c), respectively.	4
Table S1.	Crystal structure data of $CoTPP(NO_2)Cl_7$, $NiTPPCl_8$, $ZnTPP(NO_2)Cl_7$, and $ZnTPPCl_8$.	5
Table S2.	Selected average bond lengths and bond angles of $CoTPP(NO_2)Cl_8$.MeOH (**1a**).MeOH, $NiTPPCl_8$(**2b**), $ZnTPP(NO_2)Cl_7$.MeOH, $ZnTPP(NO_2)Cl_7$.Py, and $ZnTPPCl_8$(2d).	6
Figs. S4 and S5	The ^1H NMR spectrum of Ni(II) complexes of synthesized compounds in $CDCl_3$ at 298 K.	7
Figs. S6-S9	The ESI-MS spectra of (**2a**)- (**2d**) in CH_3CN at 298 K.	8-9
Fig. S10	Electronic absorption spectra of (a) **1a** and **2a**, (b) **1b** and **2b**, and (c) **1c** and **2c** in toluene at 298K	10
Fig. S11	Comparative Cyclic voltammograms of (a) **1b** and **2b**, (b) **1c** and **2c** in CH_2Cl_2 under argon at room temperature.	11
Fig. S12	Axial ligation of pyridine to **2d** in toluene at 298K.	11
Figs. S13 and S14	The axial ligation studies of **1d** and **2d** with X^- (where X = CN^-, OAc^-, F^- and PO_4-) in toluene at 298K.	12-13
Figs. S15	Constructed Benesi-Hildebrand plots for **1d** and **2d** with cyanide ion in 1:1 stoichiometric ration	14

Fig. S16	The colorimetric changes of **2a** with tested anions (Top) and UV-visible spectral changes upon addition of excess of anions in the form of their TBA salts in toluene at 298 K (Bottom).	14
Fig. S17	The UV-Visible spectral titration of **2a** upon sequential addition of cyanide ion in toluene at 298 K. Insight shows a plot between $[CN^-]^2$ and $[CN^-]^2/\Delta A$.	15
Fig. S18	DPV (in V *vs* Ag/ AgCl) traces recorded for **2a** and **2a**.CN^- in CH_2Cl_2 at 298 K.	15
Fig. S19	DPV titrations of **1a** and **2a** while increasing the concentration of CN^- ion in CH_2Cl_2 containing 0.1 M $TBAPF_6$ at 298K.	16
Fig. S20	The ratiometric absorbance changes (A_{483}/A_{440}) of **2**a (1.01×10^{-5} M) on addition of 1-2eq. of CN^- and 10 eq. of other anions.	16
Fig. S21	Reversible studies of **2a** using 1mM solution of TFA in toluene at 298K.	17
Fig. S22	Fully optimized geometries of (a) top and side views of $ZnTPP(NO_2)Cl_7$ (**1d**), (b) top and side views of $ZnTPPCl_8$ (**2d**).	17
Fig. S23	Fully optimized geometries of (a, and c) top and side views of $CoTPPCl_8$ (**2a**), (b and d) top and side views of $CoTPPCl_8$**.**CN^- (**2a.**CN^-).	18
Fig. S24-S26	Frontier molecular orbitals of **1d** and **2d**, **1a** and **2a**; and **1a**.CN^- and **2a**.CN^-.	18-19
Fig. S27	Theoretical UV-Visible spectra of (a) **1a** and (b) **2a** obtained by TD-DFT calculations in gas phase.	20
Fig. S28, S29	Experimental and theoretical UV-Vis. spectra of **1a**.CN^- and **2a**.CN^- obtained from TD-DFT.	21

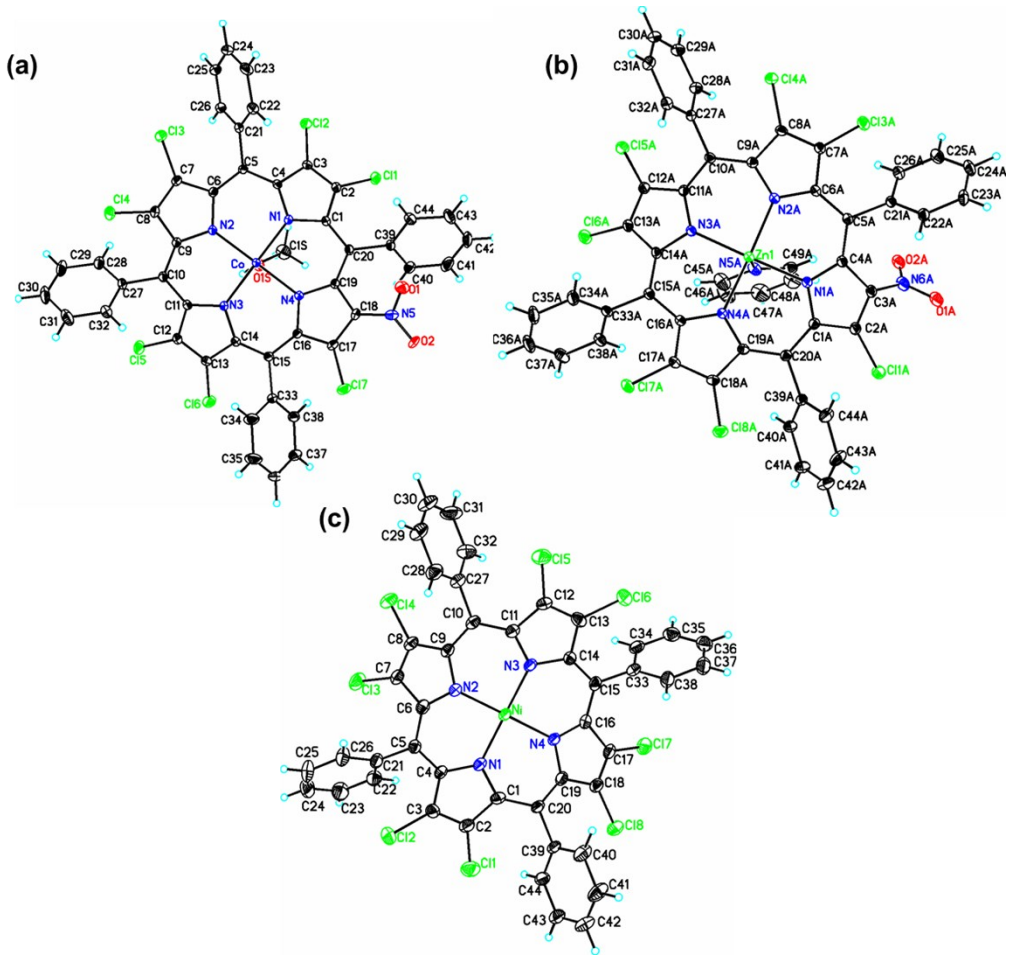

Figure S1. The ORTEP diagrams showing top views of (a) $CoTPP(NO_2)Cl_7$.MeOH (**1a**.MeOH), (b) $ZnTPP(NO_2)Cl_7$.Py (**1d**.py) and (C) $NiTPPCl_8$ (**2b**) .

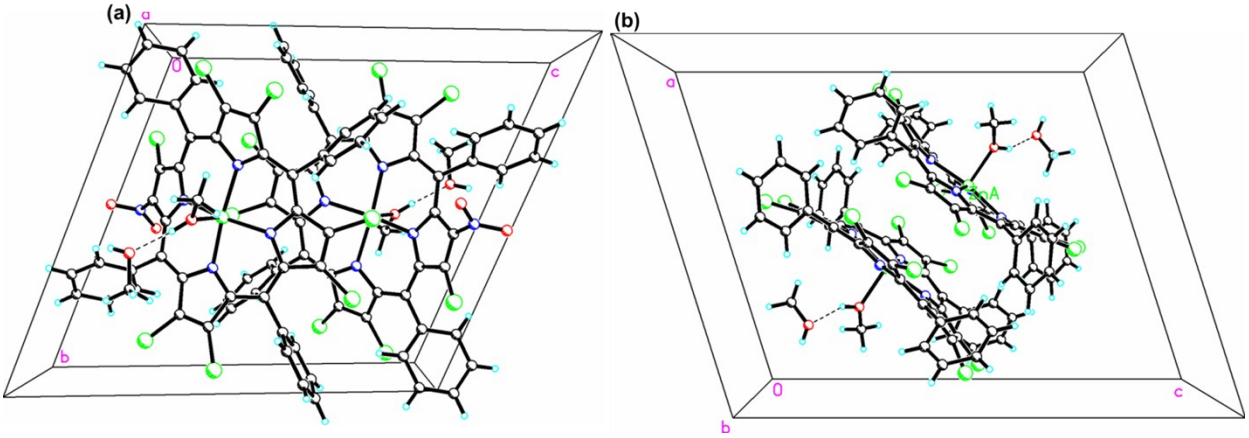

Figure S2. The packing diagram of (a) $ZnTPP(NO_2)Cl_7$.MeOH (**1d**.MeOH) and (b) $ZnTPPCl_8$.MeOH (**2b**.MeOH).

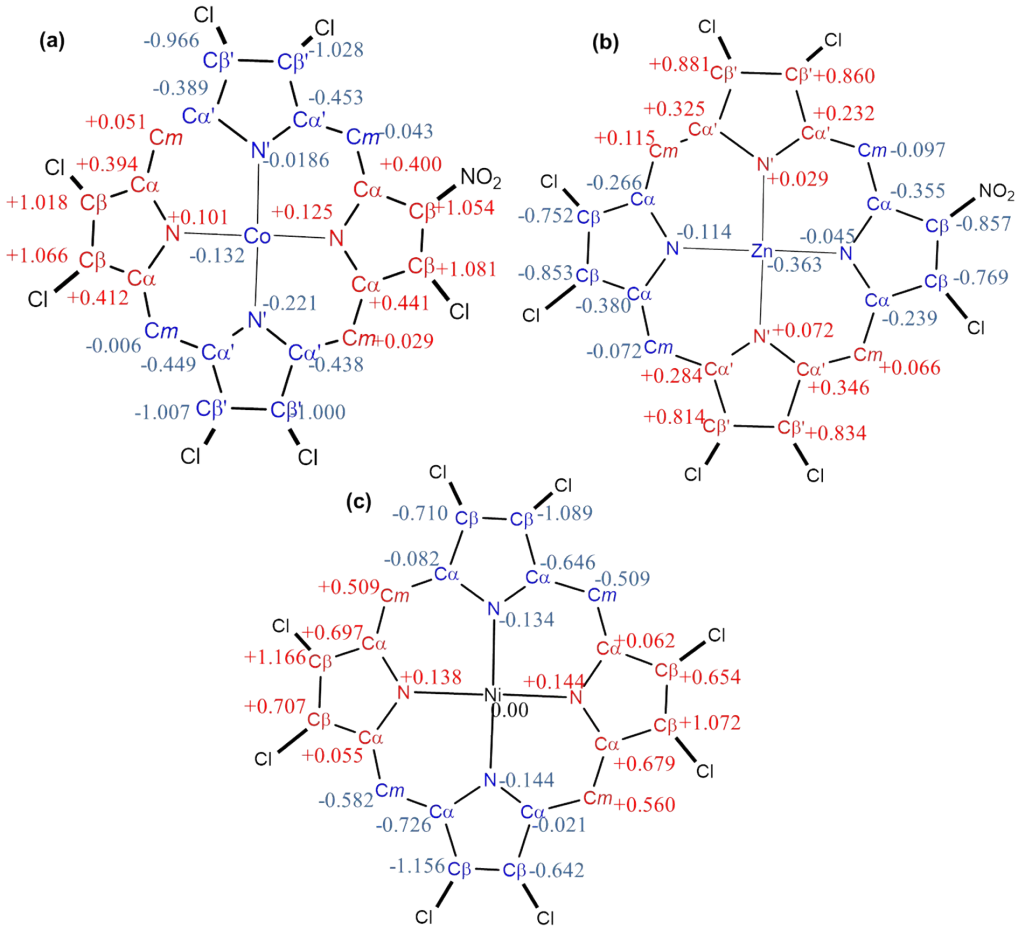

Figure S3. Displacement of porphyrin core atoms (in Angstroms) from the mean plane for $CoTPP(NO_2)Cl_7$.MeOH(**1a**.MeOH) (a), $ZnTPP(NO_2)Cl_7$.Py (**1d**.Py) and $NiTPPCl_8$ (2b) (c), respectively.

Table S1. Crystal structure data of $CoTPP(NO_2)Cl_7$, $NiTPPCl_8$, $ZnTPP(NO_2)Cl_7$, and $ZnTPPCl_8$

	$CoTPP(NO_2)Cl_7$	$NiTPPCl_8$	$ZnTPP(NO_2)Cl_7$ .Py	$ZnTPP(NO_2)Cl_7$. MeOH	$ZnTPPCl_8$ .MeOH
Empirical formula	$C_{46}H_{28}Cl_7N_5O_4Co$	$C_{44}H_{20}Cl_8N_4Ni$	$C_{49}H_{25}Cl_7N_6O_2$ Zn	$C_{46}H_{28}Cl_7.5N_4$ $.5O_3Zn$	$C_{46}H_{28}Cl_8N_4O_2Zn$
Formula wt.	1021.81	946.95	1043.27	1022.97	1017.69
Crystal system	Monoclinic	Monoclinic	monoclinic	triclinic	monoclinic
Space group	P 21/n	P 21/n	P 21/c	P -1	P 21/n
a (Å)	16.157(2)	14.4657(7)	22.161(7)	10.4998(7)	15.706(3)
b (Å)	13.9906(17)	27.0627(14)	14.459(4)	14.4853(9)	14.352(3)
c (Å)	20.088(3)	10.7356(6)	29.775(9)	15.9272(11)	19.961(4)
α (º)	90.00	90.00	90.000(5)	110.246(6)	90°
β (º)	110.01(6)	111.244(3)	105.085(12)	97.020(6)	107.639°(11)
γ (º)	90.00	90.00	90.000(5)	103.619(5)	90°
Volume ($Å^3$)	4266.8(10)	3917.2(4)	9212(5)	2153.0(3)	4288.2(15)
Z	4	4	8	2	4
Dcald (mg/m^3)	1.591	1.606	1.504	1.578	1.576
λ (Å)	0.71073	0.71073	0.71073	0.71073	0.71073
T (K)	100(2)	100(2)	100(2)	100(2)	296(2)
No. of total reflns.	52971	27312	71991	10605	61532
No. of indepnt. reflns.	8341	6843	16976	10605	11675
R	0.0538	0.0939	0.0484	0.1121	0.0444
Rw	0.0932	0.1355	0.1054	0.2957	0.1040
GOOF	1.017	1.024	1.026	1.142	1.016
CCDC	**1585103**	**1585104**	**1585105**	**1585106**	**1585107**

Table S2. Selected average bond lengths and bond angles of $CoTPP(NO_2)Cl_8$.MeOH (**1a**).MeOH, $NiTPPCl_8$(**2b**), ZnTPP(NO2)Cl7.MeOH, ZnTPP(NO2)Cl7.Py, and $ZnTPPCl_8$(2d).

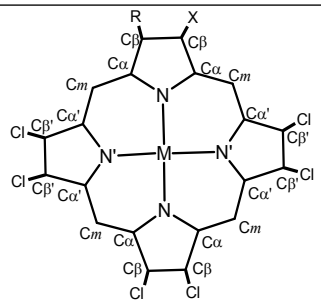

R = NO_2, $MTPP(NO_2)Cl_7$
R = Cl, $MTPPCl_8$

	$CoTPP(NO_2)Cl_7$ (**1a**)	$NiTPPCl_8$ (**2b**)	$ZnTPP(NO_2)Cl_7$ (**1d**).**MeOH**	$ZnTPP(NO_2)Cl_7$ (**1d**).**Py**	$ZnTPPCl_8$ (**2d**)
	Bond Lengths (Å)				
M -N	1.959(2)	1.906(4)	2.057(4)	2.095(3)	2.075(4)
M -N′	1.945(2)	--	2.089(5)	2.099(3)	--
N -C_α	1.379(4)	1.386(5)	1.373(6)	1.379(4)	1.378(4)
N′-C_α'	1.373(3)	--	1.369(5)	1.384(4)	--
C_α -C_β	1.441(3)	1.444(6)	1.448(7)	1.455(4)	1.452(4)
C_α'-C_β'	1.439(3)	--	1.439(6)	1.454(4)	--
C_β- C_β	1.340(3)	1.344(6)	1.323(9)	1.355(5)	1.353(4)
C_β'-C_β'	1.341(3)	--	1.332(8)	1.356(4)	--
C_α-C_m	1.393(3)	1.393(6)	1.401(8)	1.412(4)	1.406(4)
C_α'-C_m	1.393(3)	--	1.388(7)	1.417(4)	--
ΔC_β[a]	**1.028**	**0.899**	**0.706**	**0.827**	**0.642**
Δ24[b]	**0.515**	**0.536**	**0.343**	**0.402**	**0.313**
ΔM	**0.132**	**0.00**	**0.305**	**0.363**	**0.228**
	Bond Angles (º)				
N- M-N	165.59(8)	171.60(1)	162.09(2)	164.50(1)	166.96(9)
N′-M-N′	175.79(8)	--	167.39(2)	158.90(1)	--
M -N-C_α	125.10(1)	125.20(3)	125.04(4)	122.10(2)	123.93(2)
M -N′-C_α'	125.20(2)	--	123.14(4)	125.12(2)	--
N- C_α-C_m	123.89(2)	123.79(4)	125.68(5)	124.48(3)	125.11(4)
N′-C_α'-C_m	123.64(2)	--	124.72(5)	124.92(3)	--
N-C_α -C_β	108.37(2)	108.23(4)	107.15(5)	107.90(3)	108.06(2)
N′-C_α'-C_β'	108.57(2)	--	106.93(5)	107.84(3)	--
C_β -C_α -C_m	127.37(2)	127.21(4)	126.98(5)	127.40(3)	126.67(3)
C_β'-C_α'-C_m	127.16(2)	--	127.74(5)	127.09(3)	--
C_α -C_β -C_β	107.79(2)	107.80(4)	108.33(5)	107.70(3)	107.69(3)
C_α'-C_β'- C_β'	107.54(2)	--	108.09(5)	107.83(3)	--
C_α -N-C_α	107.19(2)	107.20(3)	108.86(5)	108.56(3)	108.33(2)
C_α'- N′- C_α'	107.05(2)	--	108.79(5)	108.48(3)	--
C_α -C_m -C_α'	121.28(2)	119.99(4)	124.59(5)	124.04(3)	125.10(3)

[a]ΔC_β refers to the mean plane deviation of the β-pyrrole carbons
[b] Δ24 refers to the mean plane deviation of 24 core atoms

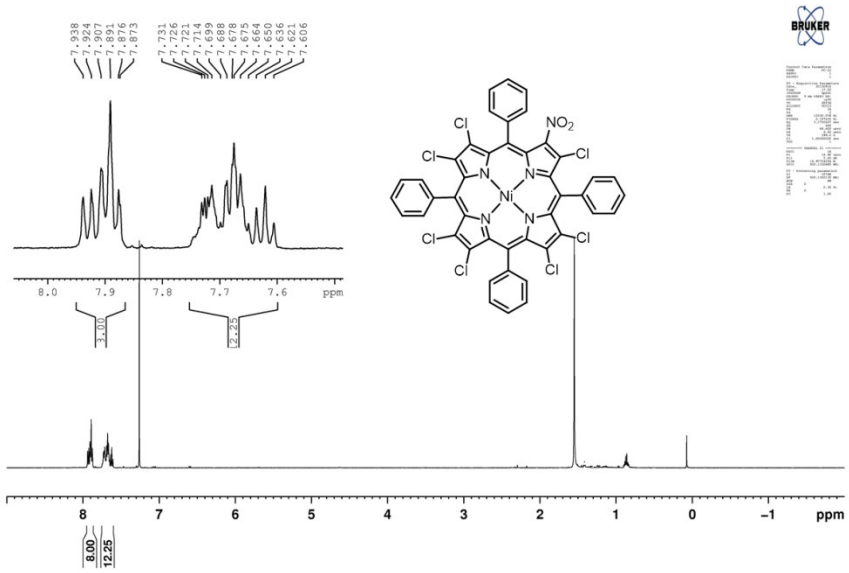

Figure S4. ^{1}H NMR spectrum of $NiTPPNO_2Cl_7$ (**2a**) in $CDCl_3$ at 298 K.

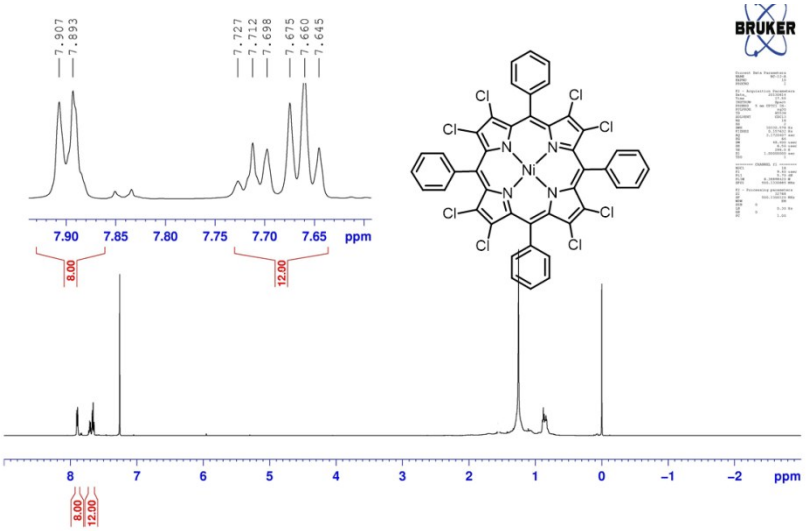

Figure S5. ^{1}H NMR spectrum of $NiTPPCl_8$ (**2b**) in $CDCl_3$ at 298 K.

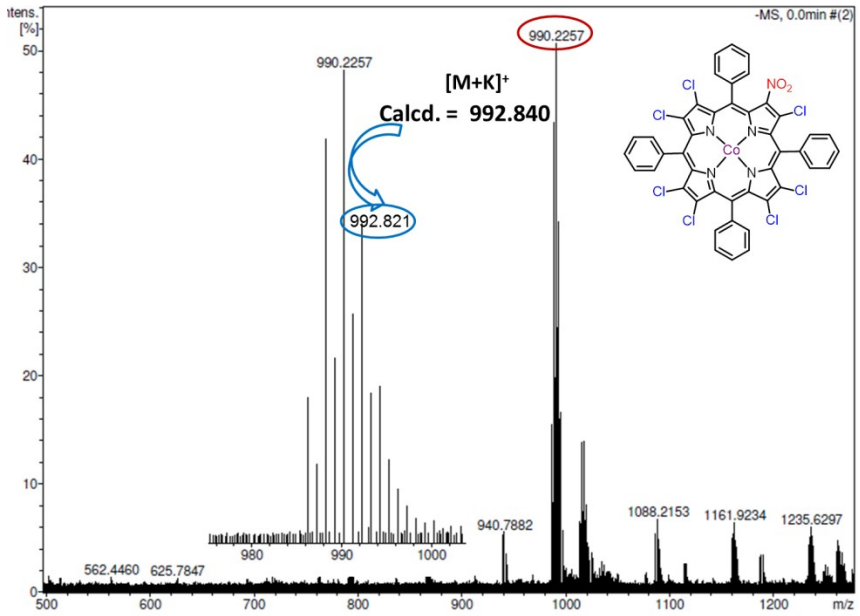

Figure S6. The ESI-MS spectra of $CoTPP(NO_2)Cl_7$ (**2a**) in CH_3CN at 298 K.

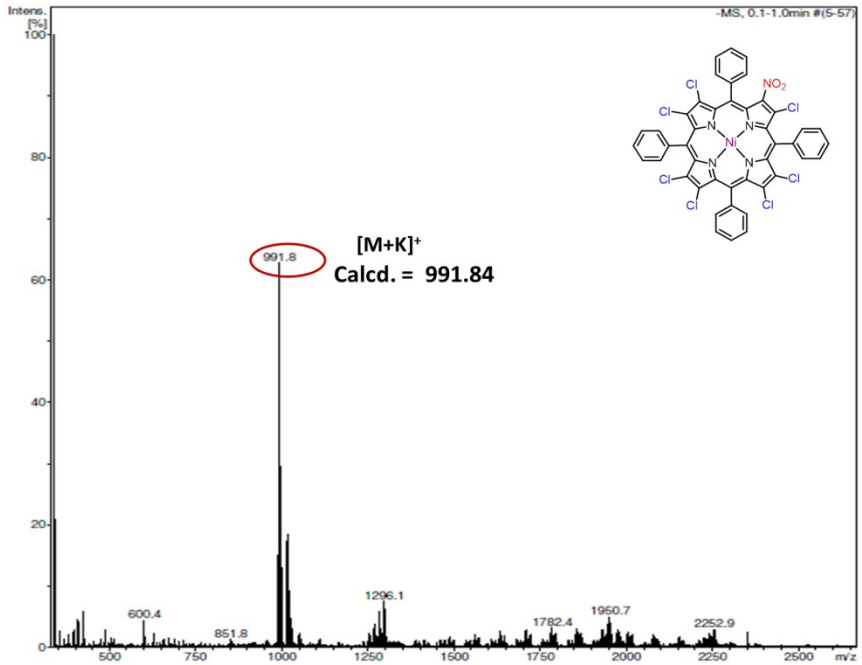

Figure S7. The ESI-MS spectra of $NiTPP(NO_2)Cl_7$ (**2b**) in CH_3CN at 298 K.

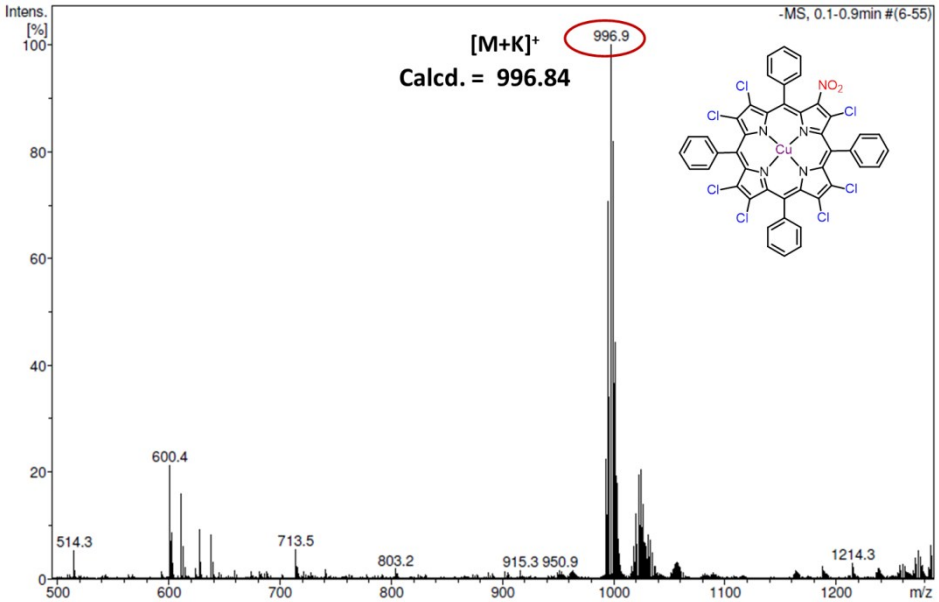

Figure S8. The ESI-MS spectra of CuTPP(NO_2)Cl_7 (**2c**) in CH_3CN at 298 K.

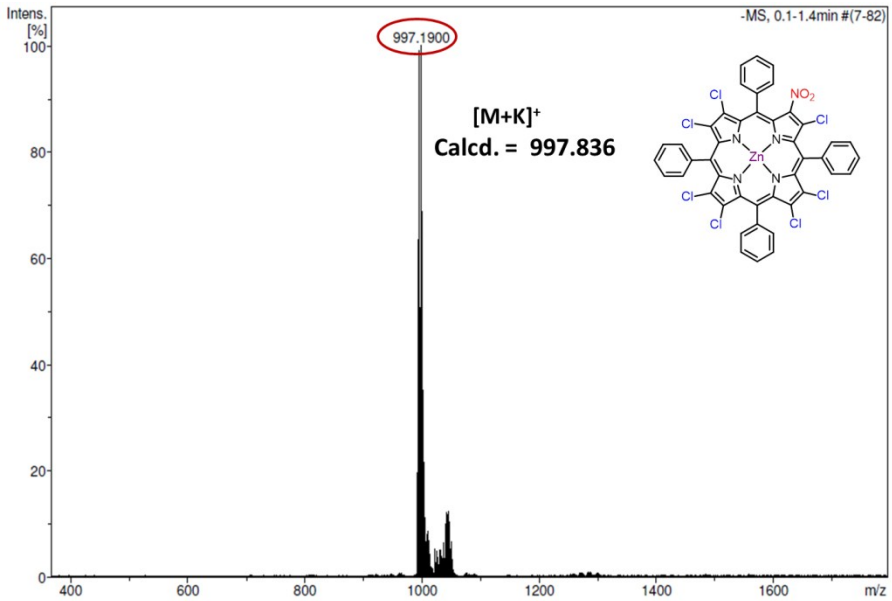

Figure S9. The ESI-MS spectra of ZnTPP(NO_2)Cl_7(**2d**) in CH_3CN at 298 K.

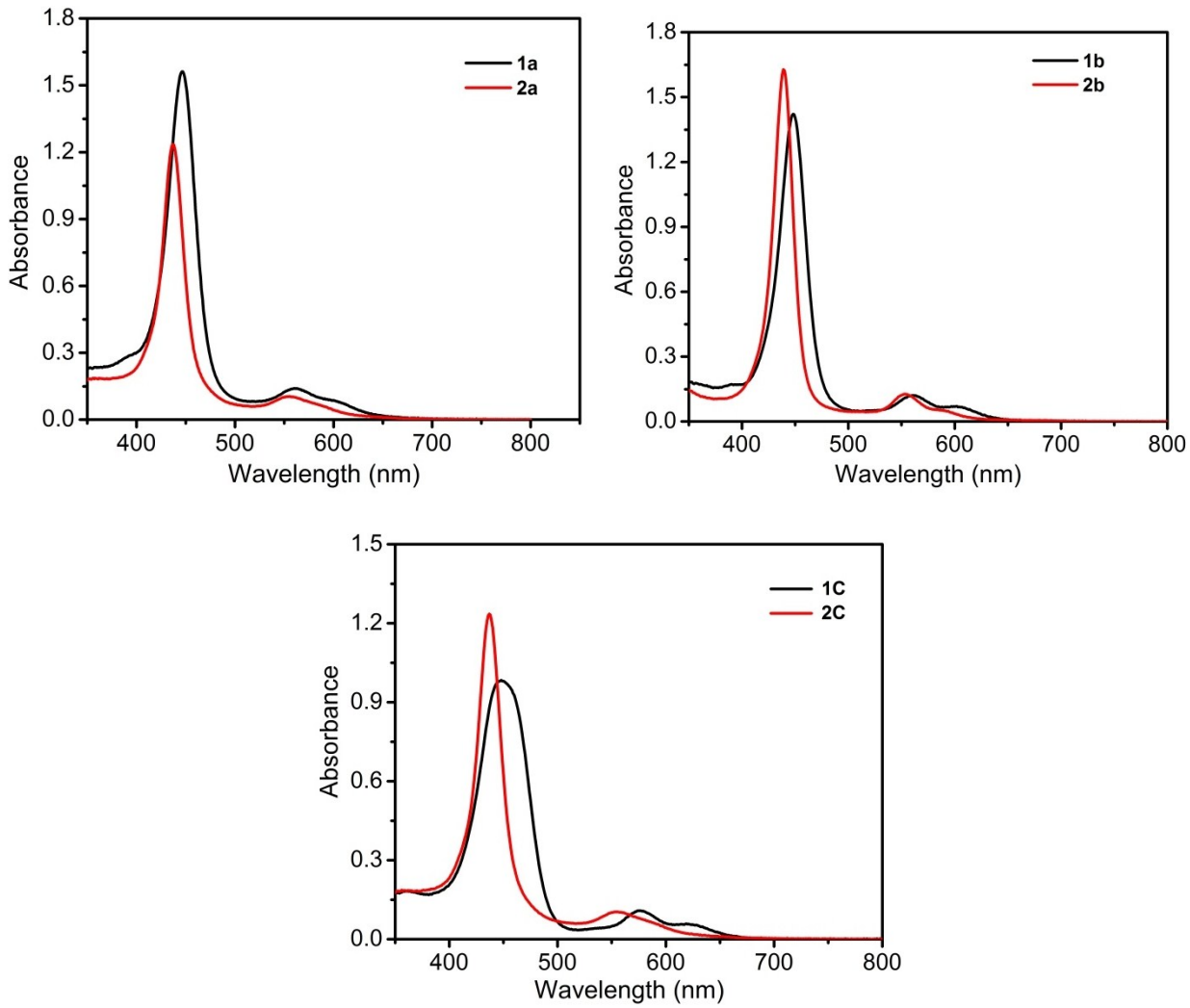

Figure S10. Electronic absorption spectra of (a) **1a** and **2a**, (b) **1b** and **2b**, and (c) **1c** and **2c** in toluene at 298K

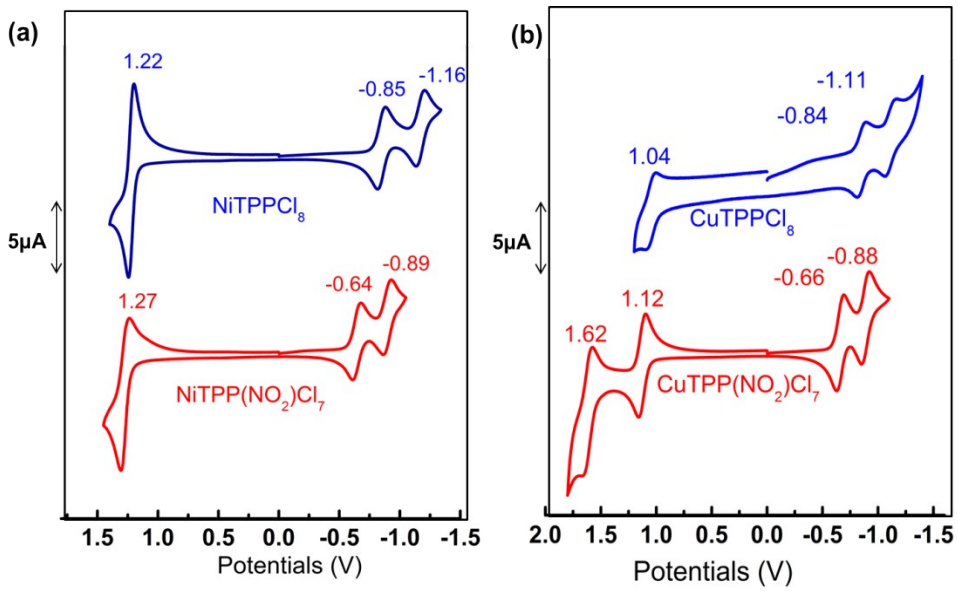

Figure S11. Comparative Cyclic voltammograms of (a) **1b** and **2b**, (b) **1c** and **2c** in CH_2Cl_2 under argon at room temperature with 0.1M $TBAF_6$ as the supporting electrolyte at a scan rate of 100 mV/s.

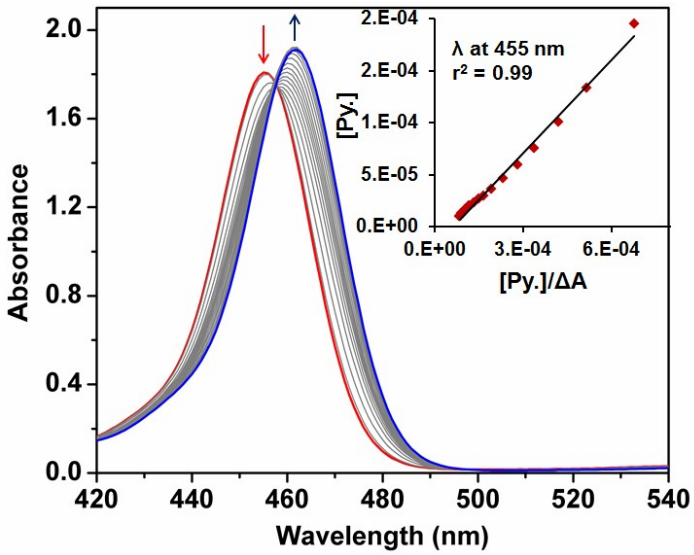

Figure S12. Axial ligation of pyridine to **2d** in toluene at 298K.

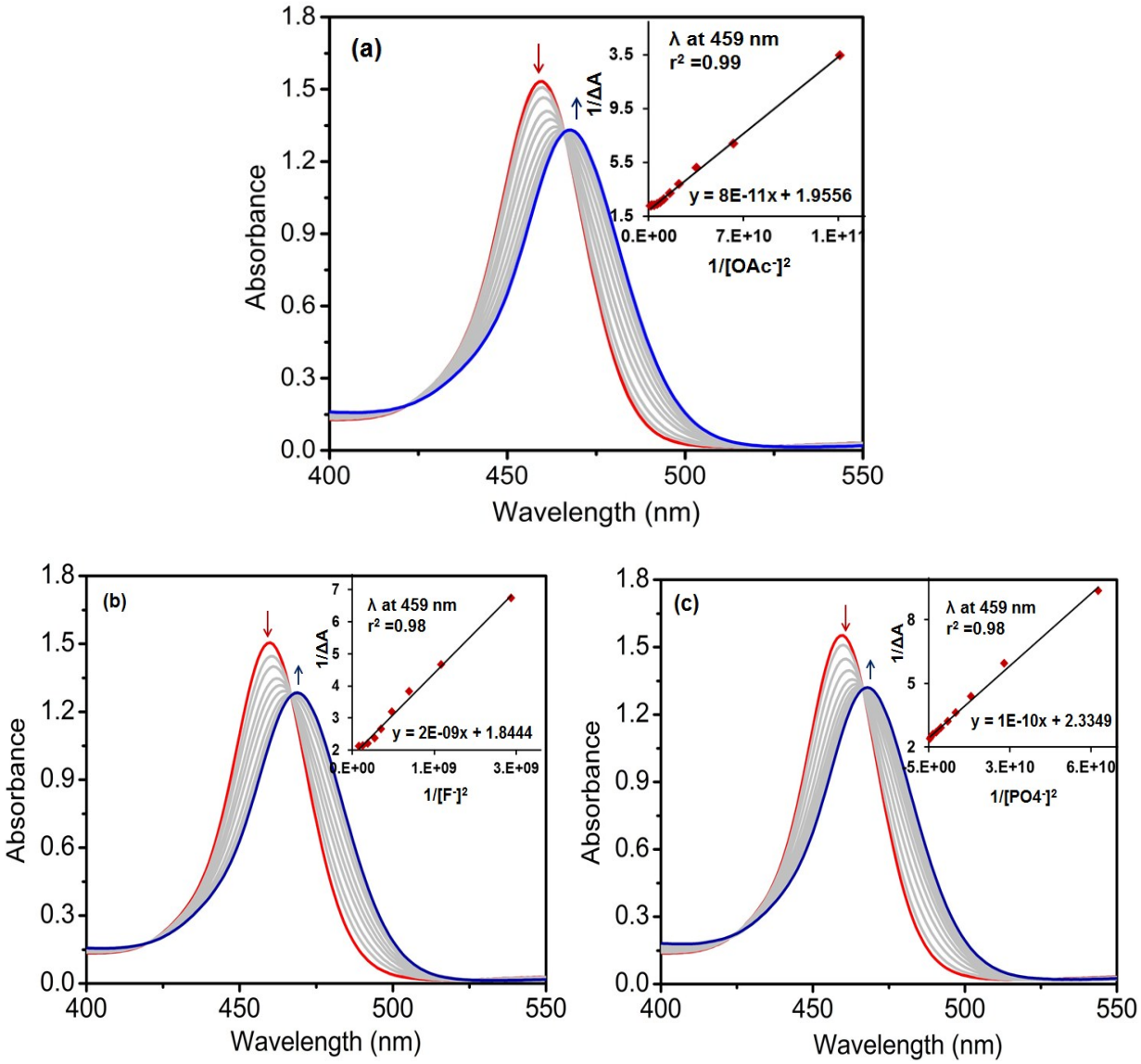

Figure S13. The axial ligation studies of X^-, Where X = OAc^- (a), F^- (b), and PO_4^- (c) anions to **1d** (8.29×10^{-6} M) in toluene at 298K. Main plots show the spectral changes in Soret region and insets show plot $[X^-]^2$ VS $[X^-]^2/\Delta A$.

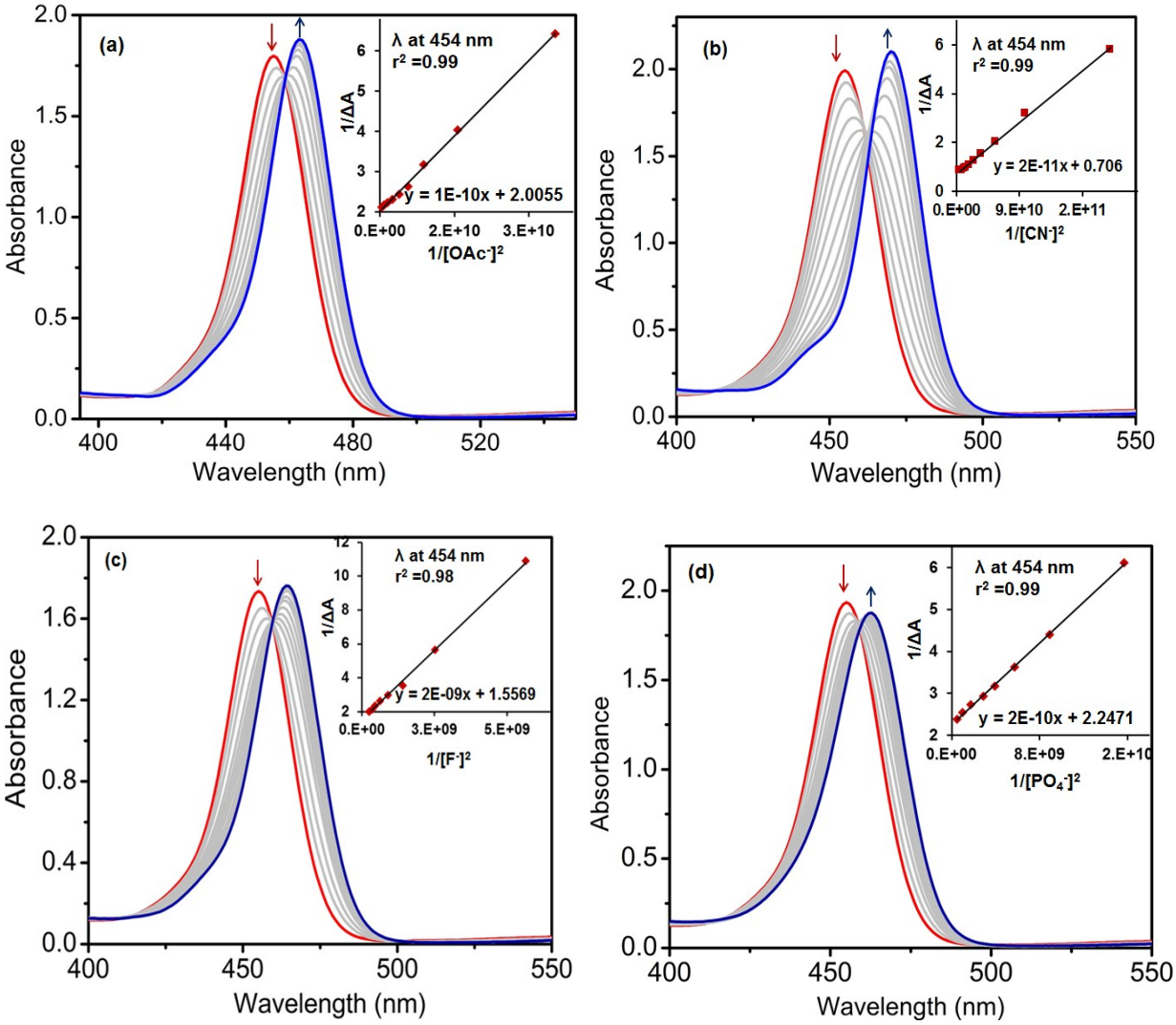

Figure S14. The axial ligation studies of X^- Where X = OAc^- (a), CN^- (b), F^- (c) and PO_4^- (d) anions to **2d** (8.38×10^{-6} M) in toluene at 298K. Main plots show the spectral changes in Soret region and insets show plot $[X^-]^2$ VS $[X^-]^2/\Delta A$.

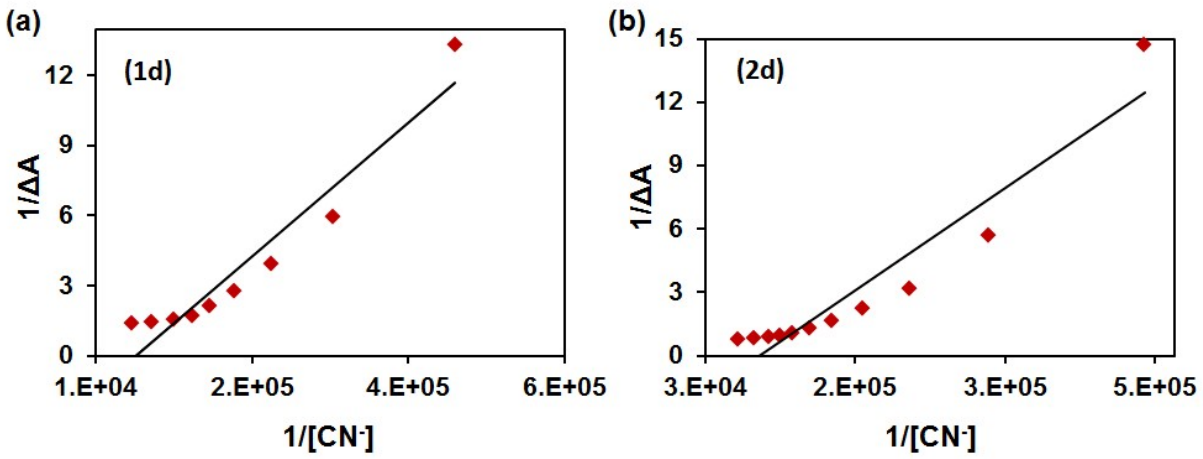

Figure S15. Benesi-Hildebrand plot constructed for 1:1 stoichiometric ratio from the titration data of **1d** and **2d** with cyanide ion. Cyanide binding is not accurately modeled by this plot indicating that binding cannot be of 1:1 stoichiometry.

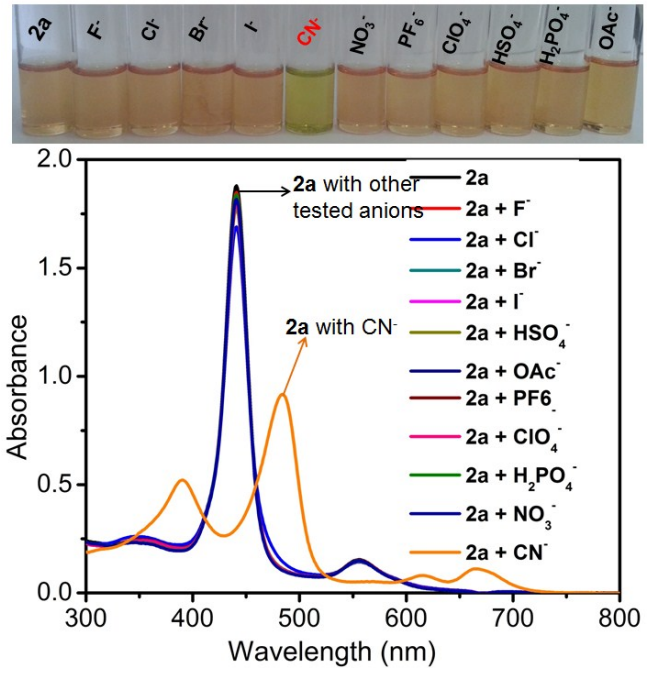

Figure S16. The colorimetric changes of **2a** with tested anions in toluene at 298K (Top). The UV-visible spectral changes of **2a** upon addition of excess of anions in the form of their TBA salts in toluene at 298 K (Bottom).

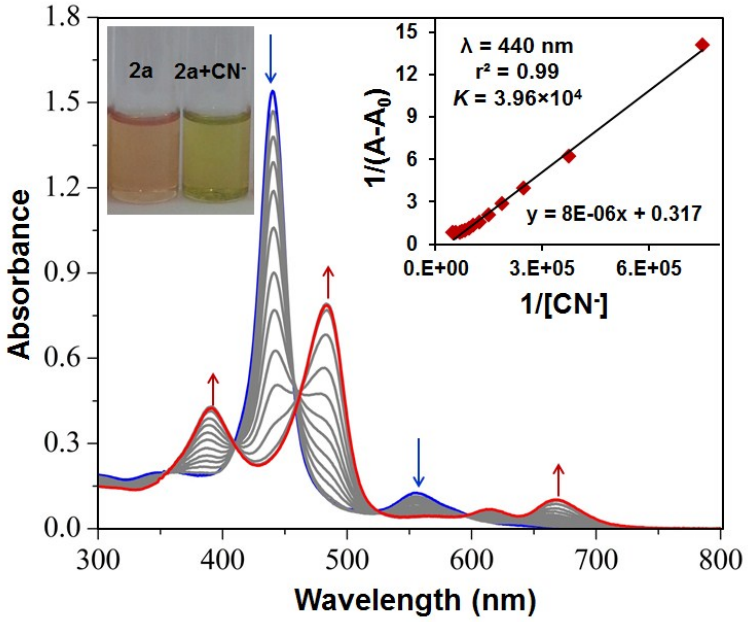

Figure S17. The UV-Visible spectral titration of **2a** (1.05×10^{-5} M) upon sequential addition of cyanide ion in toluene at 298 K. Insight shows BH plot between 1/ΔA and 1/[CN^-].

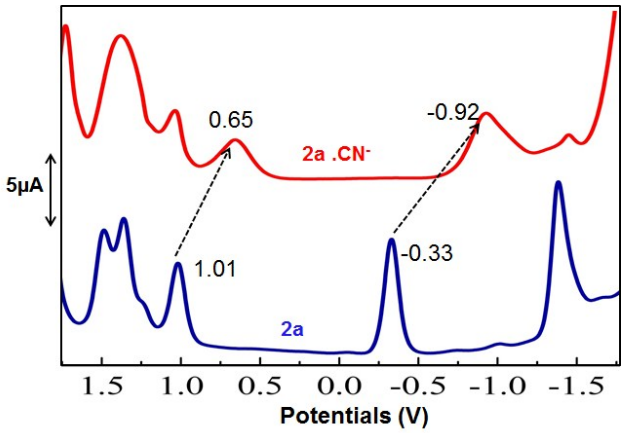

Figure S18. DPV (in V *vs* Ag/ AgCl) traces recorded for **2a** and **2a**.CN^- in CH_2Cl_2 containing 0.1M $TBAPF_6$ with a scan rate of 0.1 Vs^{-1} at 298 K.

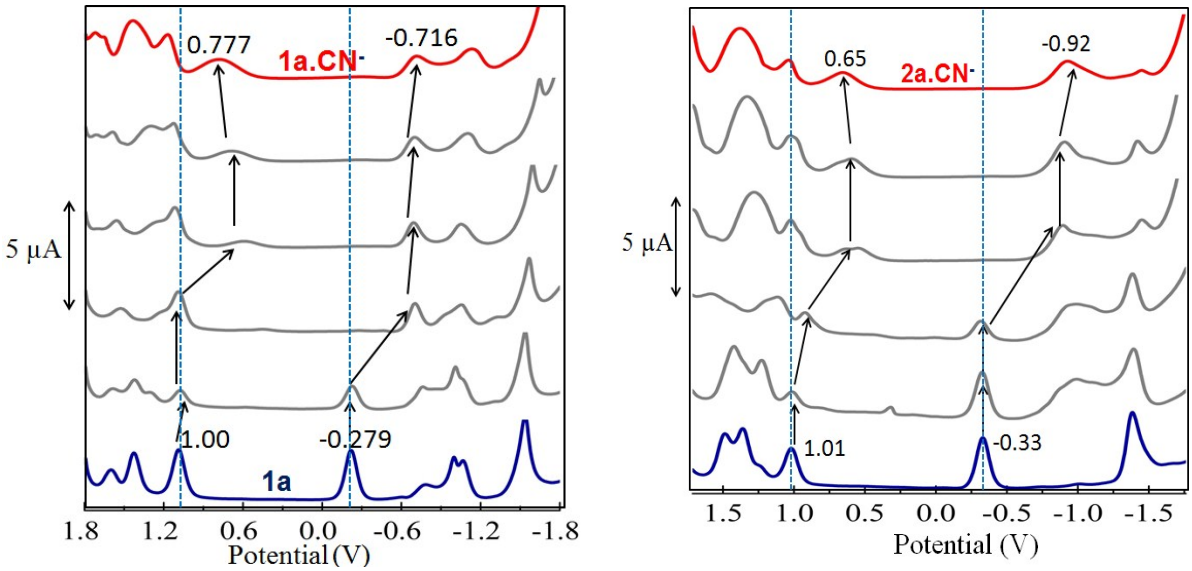

Figure S19. DPV titrations of **1a** and **2a** while increasing the concentration of CN^- ion in CH_2Cl_2 containing 0.1 M $TBAPF_6$ at 298K.

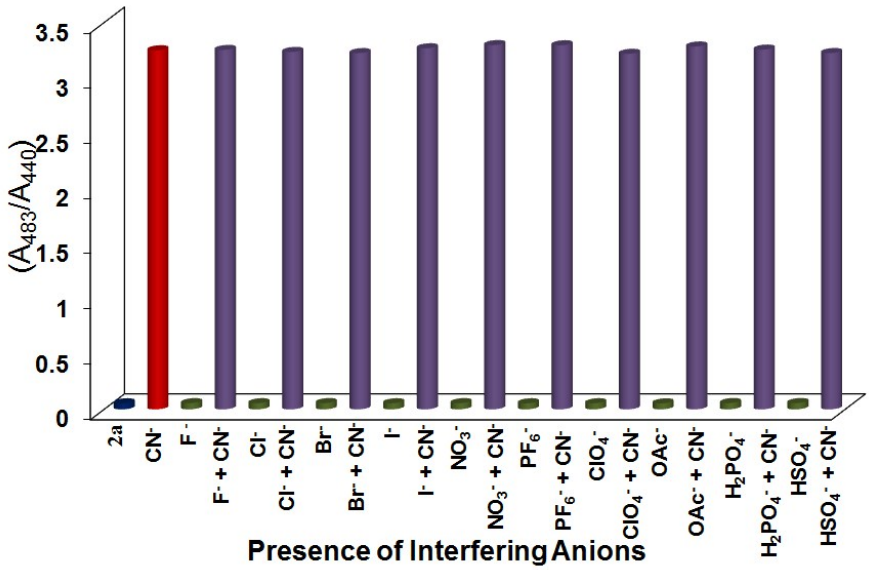

Figure S20. The ratiometric absorbance changes (A_{483}/A_{440}) of **2**a (1.05×10^{-5} M) on addition of 2 eq. of CN^- and 10 eq. of other anions. Green bars indicate the blank and in presence of other interfering anions, and purple bars indicate the addition of CN^- to the interfering anions.

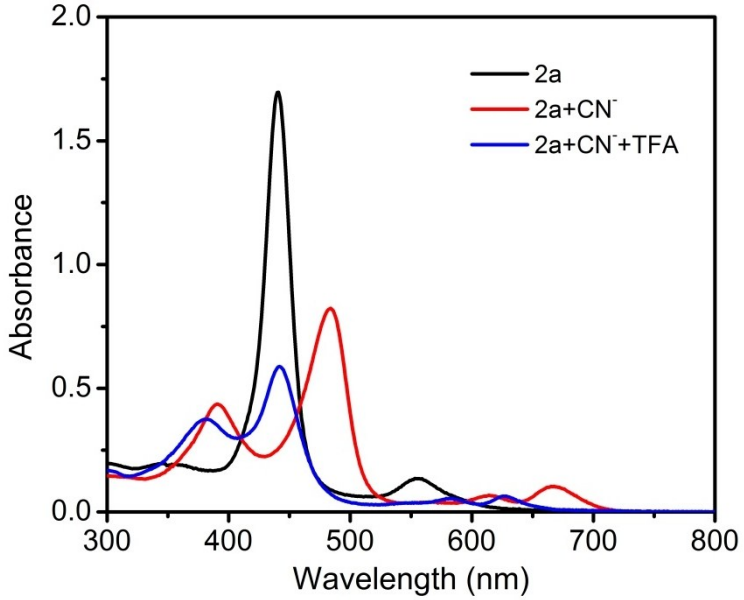

Figure S21. Reversible studies of **2a** using 1mM solution of TFA in toluene at 298K.

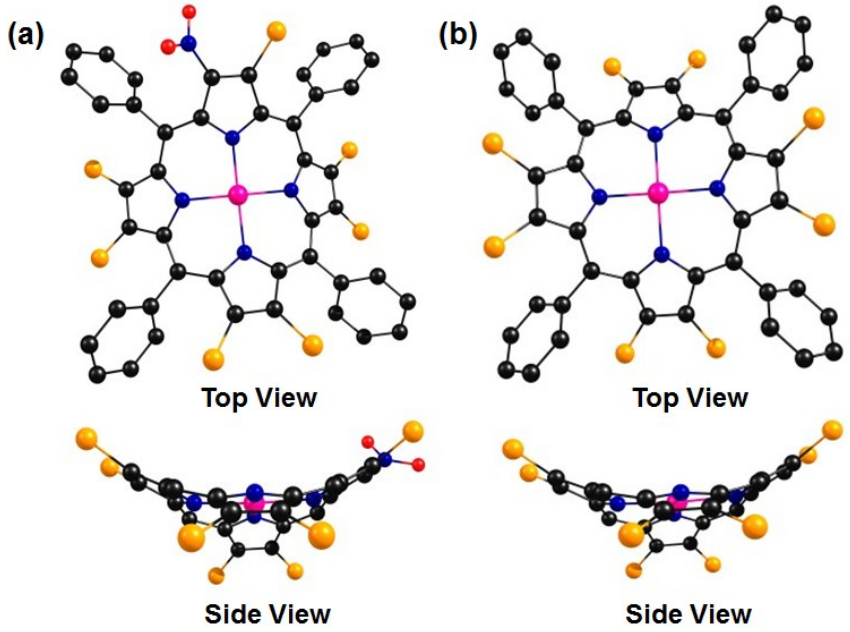

Figure S22. Fully optimized geometries of (a) top and side views of ZnTPP(NO_2)Cl_7 (**1d**), (b) top and side views of ZnTPPCl_8 (**2d**) .H atoms in top views and phenyl rings in side views are omitted for clarity.

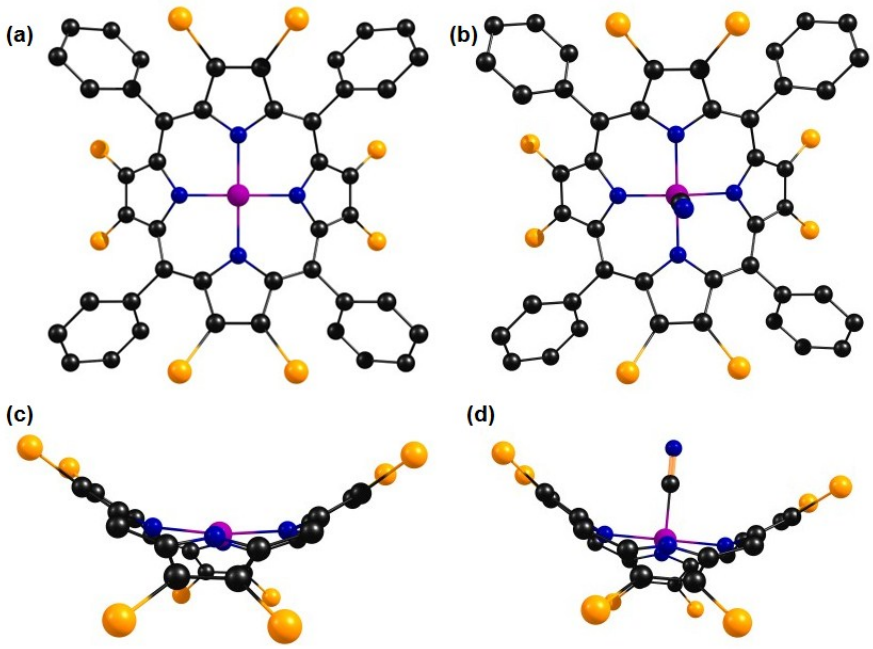

Figure S23. Fully optimized geometries of (a and c) top and side views of $CoTPPCl_8$ (**2a**), (b and d) top and side views of $CoTPPCl_8$**.**CN^- (**2a.**CN^-) .H atoms in top views and phenyl rings in side views are omitted for clarity.

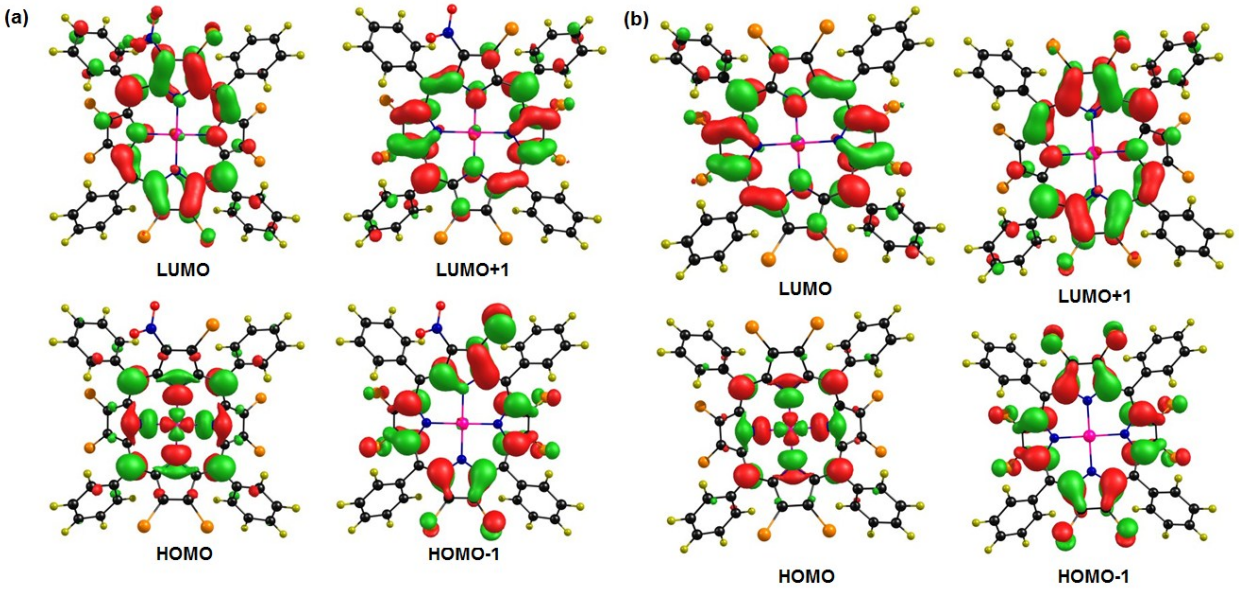

Figure S24. The Pictorial representation of frontier molecular orbitals of (a) $ZnTPP(NO_2)Cl_7$ (**1d**) and, (b) $ZnTPPCl_8$ (**2d**).

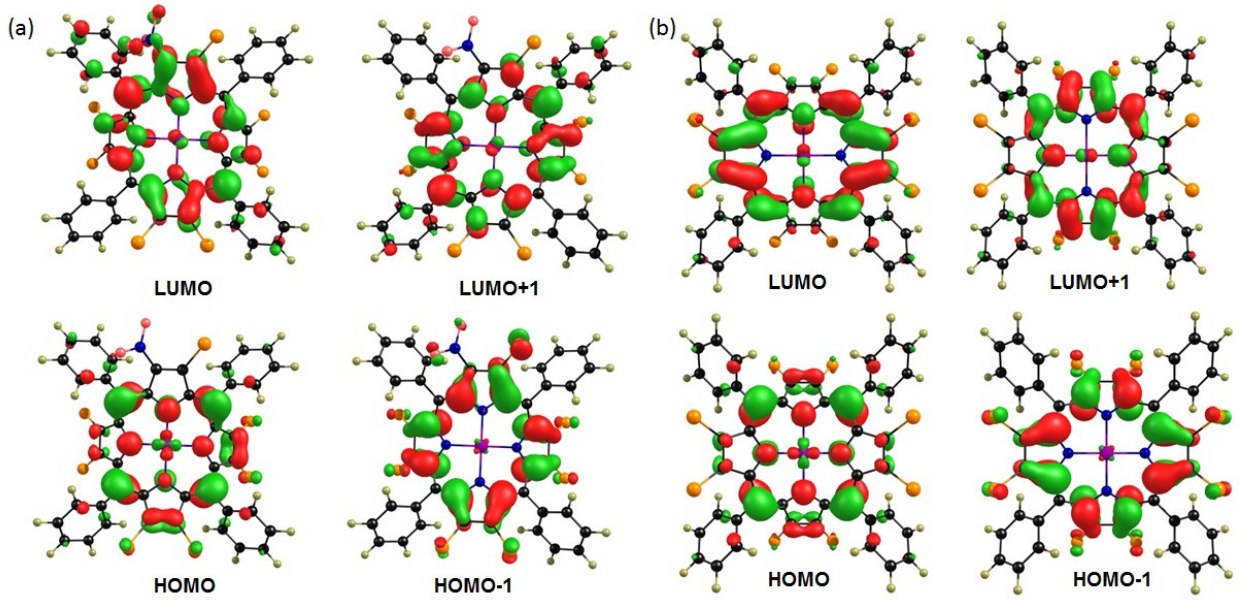

Figure S25. The Pictorial representation of frontier molecular orbitals of (a) $CoTPP(NO_2)Cl_7$ (**1a**) and, (b) $CoTPPCl_8$ (**2a**).

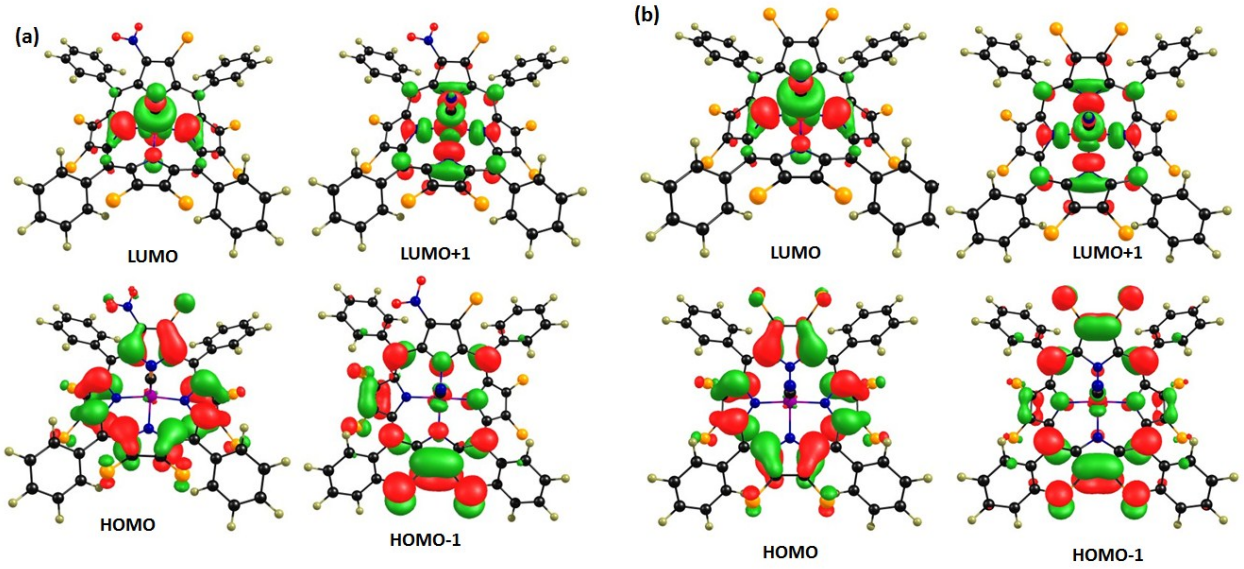

Figure S26. The Pictorial representation of frontier molecular orbitals of (a) $CoTPP(NO_2)Cl_7$ (**1a.**CN^-) and, (b) $CoTPPCl_8$ (**2a.**CN^-).

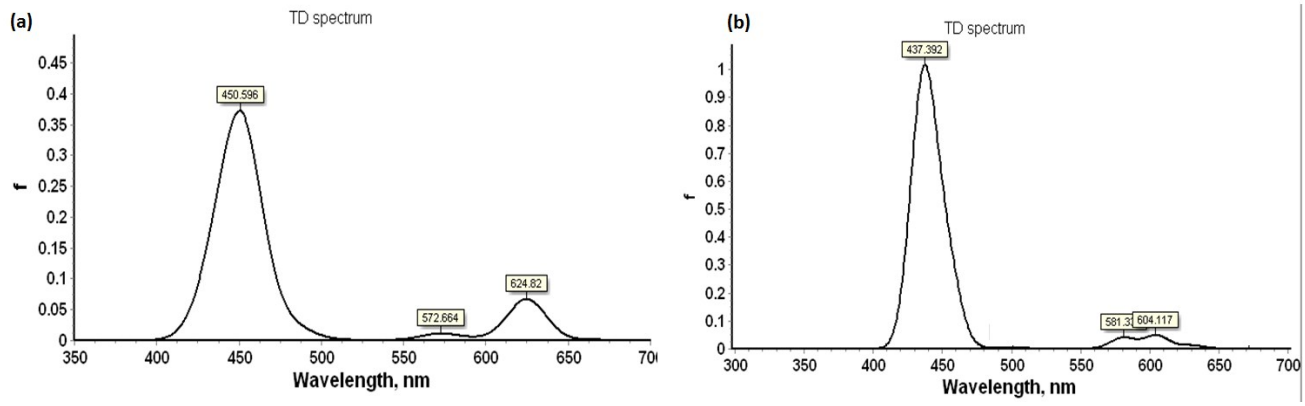

Figure S27. Theoretical UV-Visible spectra of (a) **1a** and (b) **2a** obtained by TD-DFT calculations in gas phase.

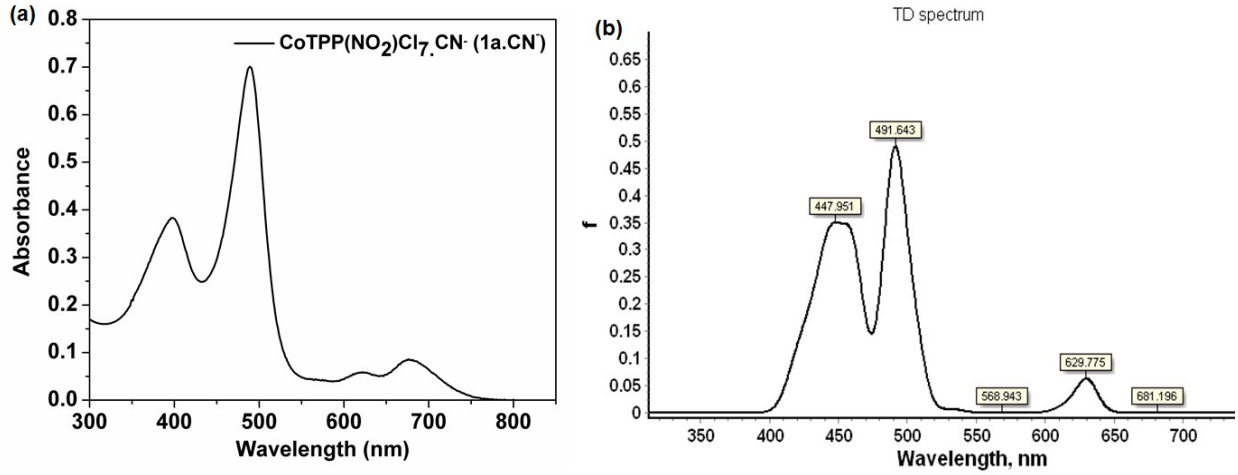

Figure S28. The comparison between (a) experimental UV-Vis spectrum and (b) The theoretical UV-Vis. spectrum of $CoTPP(NO_2)Cl_7.CN^-$ (**1a.**CN^-).

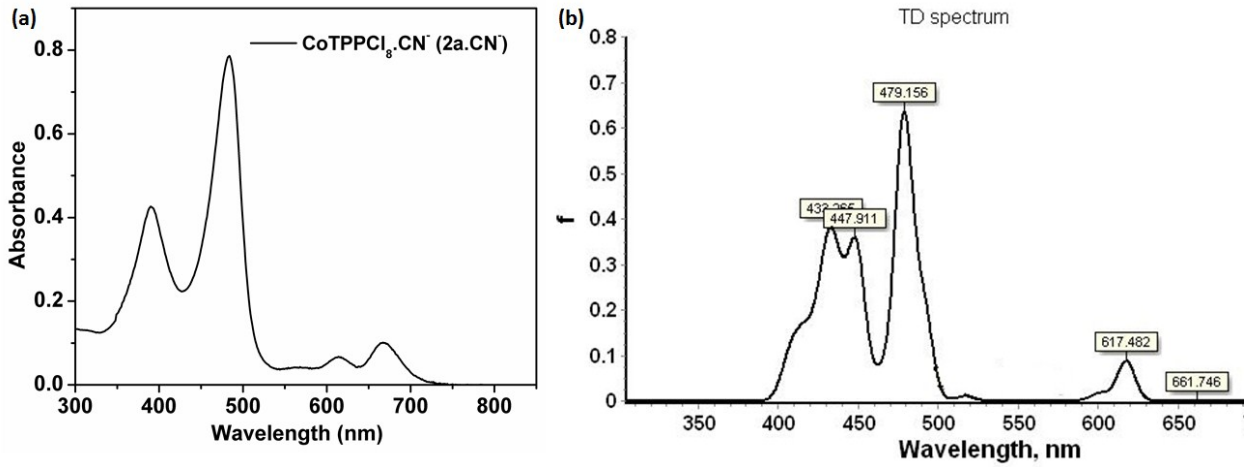

Figure S29. Experimental UV-Vis spectrum (a) and Theoretical UV-Vis. spectrum (b) of $CoTPPCl_8.CN^-$ (**2a.**CN^-).